LIMNOLOGY
and
OCEANOGRAPHY: METHODS

Limnol. Oceanogr.: Methods 7, 2009, 132–143

Improved algorithm for the computation of nitrate concentrations in seawater using an in situ ultraviolet spectrophotometer

Carole M. Sakamoto, Kenneth S. Johnson, Luke J. Coletti*
Monterey Bay Aquarium Research Institute, Moss Landing, CA, 95039 USA

Abstract

Improvements in the data processing algorithm and calibration procedures have greatly increased the accuracy of nitrate measurements using an in situ ultraviolet spectrophotometer (ISUS). Two major changes in the algorithm involve application of a temperature-dependent correction to the bromide spectrum and then using the observed temperature and salinity to subtract the bromide component before fitting nitrate. By reducing the degrees of freedom in calculating nitrate concentrations, the accuracy of the ISUS instrument is substantially improved. The new algorithm was tested in environments ranging from the Southern Ocean to oligotrophic eastern Pacific seawater and found to be applicable at all temperatures and depths. The standard error of the estimate for regression between ISUS nitrate values and discrete samples measured by standard wet chemistry methods for the combined data set is reduced by greater than 2-fold (1.4 down to 0.65 µM) using the new algorithm. This corresponds to a 5-fold reduction in variance (2.0 down to 0.4 μM^2). Although biofouling and calibration drift remain issues for any instrument deployed in situ for long periods of time, using the measured salinity and temperature to correct the ultraviolet spectra before the nitrate calculations will reduce the impacts of these confounding processes.

Introduction

Nitrate limits primary production in much of the aquatic environment. The ability to make high-resolution nitrate measurements in situ for extended periods of time is critical to assess the spatial and temporal variability due to natural and anthropogenic inputs in lakes, rivers, estuaries, and the ocean (McNeil et al. 1999, Sakamoto et al. 2004, Johnson et al. 2006). The development of an in situ ultraviolet spectrophotometer (ISUS) system with high spectral resolution (<1 nm) and short response time (<1 s) was reported in 2002 (Johnson and Coletti 2002). It was demonstrated that this instrument could be used for direct optical determinations of UV-absorbing compounds (nitrate, bromide, and bisulfide) without chemical manipulations. Nitrate measurements made with the ISUS at hourly resolution over long time periods (months to years) allow new production to be monitored directly (Johnson et al. 2006).

Although it was noted when the ISUS instrument was developed that low temperatures produced an apparent bias in the calculated salinity estimated from the bromide concentration, the impact of the effect of sample temperature on the calculated nitrate concentration was not fully appreciated (Johnson and Coletti 2002). Subsequent analyses demonstrate that the temperature dependence of bromide spectra creates a bias in nitrate measurements. This temperature induced bias is one of the main factors that limits the accuracy of the ISUS to ~ ±2 µM NO_3^-.

This article summarizes results from a series of experiments to determine a temperature correction algorithm for the ISUS that will be applicable throughout natural waters as well as improvements to the calibration procedures and data processing that increase the accuracy and performance of the instrument. Results from deployments on a conductivity, temperature, depth (CTD) rosette in the Southern Ocean, California coastal waters, and oligotrophic regions of the Pacific Ocean, as well as a year-long mooring deployment in the coastal environment, illustrate the utility and versatility of the instrument for both profiling and moored applications in coastal and oligotrophic waters. Application of the temperature corrections results in a significant increase in accuracy.

*Corresponding author: E-mail: saca@mbari.org

Acknowledgments

This work was supported by a grant from the David and Lucile Packard Foundation to the Monterey Bay Aquarium Research Institute. Thanks to H. Jannasch, M. Blum, T. Pennington, D. Conlin, the MBARI Ocean Observatory Group, and Machine Shop personnel for assistance on this project. Thanks also to the crews of the Research Vessels Point Lobos, Western Flyer, and Revelle.

Materials and procedures

Instrument description and data processing—The major components of the ISUS instrument are a Heraeus Fiberlight deuterium light source, a Zeiss MMS series photodiode array spectrometer optimized for the UV, fiber-optically coupled reflection probes from C-Technology or Equitech International, and an Onset Computer Co. model TT8V2 datalogger augmented with a Persistor Inc. model CF8V2 Compact Flash adapter. The instrument design and calculation procedures have been described in detail (Johnson and Coletti 2002). ISUS units are now commercially available, but all work reported here was done with units custom-built in our laboratory. These instruments are functionally similar to commercially available units.

The UV spectra of solutions of deionized water, oligotrophic low-nutrient seawater (<0.1 µM NO_3^- determined by an Alpkem Rapid Flow Analyzer) with a known salinity (determined by a salinometer), and the same seawater with 40 µM NO_3^- added were measured with several ISUS instruments. The solutions were temperature-regulated and pumped through a flowcell mounted on the ISUS instrument fitted with a 40-psi backpressure regulator at the outlet. The sample temperature was also measured.

The raw absorbance at each wavelength is calculated from the equation:

$$A_\lambda = -\log_{10}\left(\frac{I_\lambda - I_D}{I_{\lambda,0} - I_D}\right) \quad (1)$$

where A_λ is the absorbance at wavelength λ when I_λ is the detector intensity (counts) at wavelength λ for the sample, $I_{\lambda,0}$ is the detector intensity at wavelength λ for a deionized water (DIW) blank, and I_D is the detector dark current.

The seawater spectra in our experiments are baseline corrected in the wavelength range of 210 to 245 nm by subtracting a linear regression of absorbance versus wavelength fitted to the uncorrected absorbances from 240 to 260 nm. It is important to note that the oligotrophic seawater used for our experiments and laboratory calibrations is stored in acid-cleaned glass bottles and has not had any storage time in plastic containers (bottles, carboys, or vats). The acid-cleaned glass bottle storage requirement is necessary to maintain a low DOC concentration in the seawater. The sea salt extinction coefficients (ESW) at each wavelength are calculated by dividing the low nutrient seawater absorbance after baseline correction by the measured salinity.

The absorbance difference between the seawater solutions with and without added nitrate gives the absorbance due to the added nitrate. The nitrate extinction coefficient (ENO_3^-) is calculated by dividing the absorbance difference due to the addition of a nitrate standard by the standard concentration. All intensities were corrected for dark current using the average intensity of the first 100 pixels (~80 nm wavelength range) measured with the lamp's shutter closed. The average of only the first 100 pixels is used to eliminate any possible ambient light effects at longer UV wavelengths.

Chemical concentrations are determined using the Beer-Lambert Law:

$$A_\lambda = b(\Sigma_j \varepsilon_{\lambda,j} C_j) \quad (2)$$

where b is the path length (cm) of the probe tip, $\varepsilon_{\lambda,j}$ is the extinction coefficient of chemical species j (L mol^{-1} cm^{-1}) at wavelength λ, and C_j is the concentration (mol L^{-1}) of jth chemical species that absorbs. Seawater scans can contain a background spectrum due to dissolved organic matter (CDOM); this background spectrum is approximated by a simple linear function of wavelength at wavelengths below 245 nm, and the equation becomes

$$A_\lambda = b(\Sigma_j \varepsilon_{\lambda,j} C_j + e + f\lambda) \quad (3)$$

where e and f are baseline coefficients that can be treated as adjustable parameters. Concentrations can be determined by fitting the above equation to the observed sample absorbance spectrum with a linear, least-squares optimization (Johnson and Coletti 2002). The sample spectra are fitted using a wavelength range from 217 to 240 nm (1-cm pathlength probe tip) or 220 to 245 nm (4-cm pathlength probe tip). These fit ranges are used to reduce the interference from the presence of any CDOM by ending the fit range before the CDOM spectral peak, which is typically centered at 260 nm.

Laboratory calibration apparatus—Laboratory calibration of the ISUS instrument requires temperature control and a method for pumping solutions that does not introduce contamination from UV-absorbing compounds (Figure 1). The ISUS instrument is cooled to a constant temperature by isolating the instrument in a copper double-hulled chamber with water from a circulating water bath flowing around it and a miniature fan installed on the instrument to circulate the air in the chamber.

Cooling of the ISUS instrument is required because the Hereaus lamp generates enough heat during continuous operation to raise the internal temperature of the ISUS instrumentation when it is not surrounded by water. For a calibration, the ISUS instrument is first chilled in the chamber and then powered up and allowed to operate until the temperature stabilizes (~1 h), after which it tends to remain fairly constant (±0.2°C). For example, if the circulating water bath is set to 6°C, the ISUS internal temperature may stabilize at ~12°C.

Changes in the internal ISUS temperature do not affect the shape of the spectra. Increases in the internal instrument temperature will decrease the lamp output and increase the dark current; however, the baseline simply shifts up in a linear fashion. Because this baseline shift is a linear function of wavelength, it will appear as part of the linear instrument baseline (e and f component in Equation 3) and does not have an affect on the calculations. This is true even if the shift results in negative absorbances, which may result at internal temperatures lower than the calibration temperature.

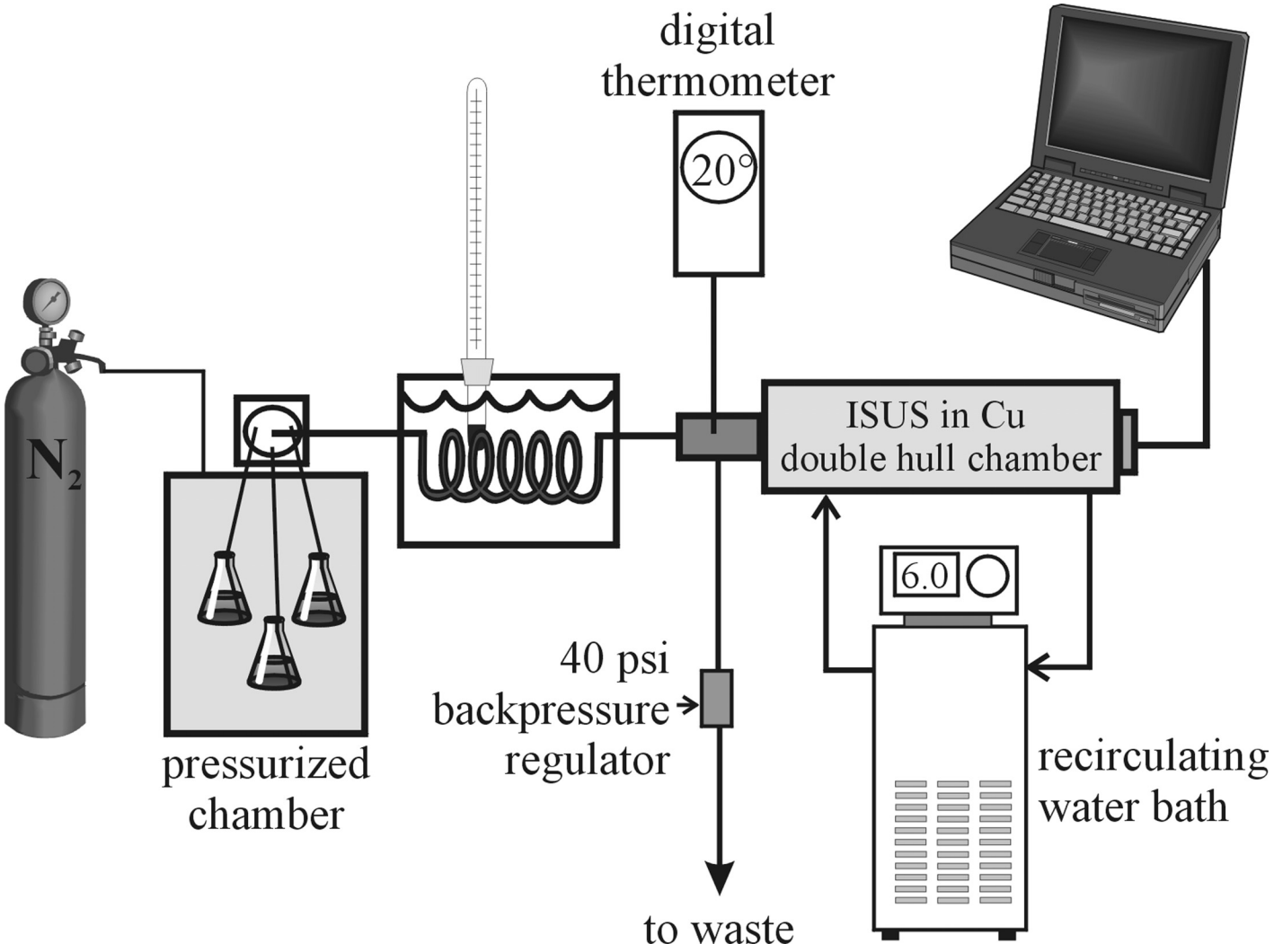

Fig. 1. Diagram of the laboratory calibration setup.

Calibrations can also be conducted by intermittently waking the instrument and taking several scans similar to the conditions during a mooring deployment. It has been observed in some laboratory experiments that calculating the seawater absorbance using a DIW scan from a continuously running instrument and an intermittently triggered seawater scan can generate small spectral peaks. It is best to match the calibration mode with the deployment mode that will be used to acquire data.

A variety of methods for pumping calibration solutions were tested to assess their performance. Contamination with DOC is evident as a broad peak near 260 nm. The most contaminant-free method was achieved by building a chamber that could be pressurized up to 60 psi with gas. The calibration solutions (DIW, low nutrient seawater with and without a known quantity of nitrate added) are held in acid-cleaned glass bottles and placed into the pressure chamber. The chamber is sealed and pressurized to 40 psi with nitrogen gas, which forces fluid through 0.8-mm i.d. PEEK tubing to a 6-port stream selection valve (Cheminert). The outlet of the stream selection valve is connected to a custom-built PEEK calibration flowcell with 220 cm of 0.8-mm i.d. PEEK tubing; 140 cm of this tubing was coiled and placed in a beaker of water that was held at different temperatures to vary the sample temperature. The temperature of the water was measured with a YSI model 4600 digital thermometer inserted into the calibration flowcell outlet. The YSI sensor is calibrated relative to NIST standards. The outlet tubing is connected to a 40-psi backpressure regulator (Upchurch Scientific, Oak Harbor, WA, USA) with 20 cm of 0.3-mm i.d. PEEK tubing added at the outlet to reduce pulsing of the flow out of the backpressure regulator (Figure 1). It is very important to pressurize the calibration solutions to eliminate any optical interference from air bubbles in the streamflow. As an important safety note, the chamber has a pressure relief valve set at 50 psi to prevent overpressurization of the chamber. As an additional safety feature, the chamber also has a steel mesh guard over the exterior to retain fragments in case of explosion due to high pressure.

Freshly dispensed DIW from a Millipore Milli-Q unit was used for spectra blanks. Pharma-80 tubing was used for the DIW dispensing tubing, as Tygon tubing will introduce contamination that appears in the UV spectra. Special care must be taken to prevent contamination from materials such as Tygon, Buna, and other plastics. The low-nutrient seawater was collected in glass jugs that had been precleaned in 10% HCl, and the calibration solutions were kept in glass bottles that had been cleaned with 10% HCl.

Assessment

Temperature experiments—The UV absorption spectrum of seawater between 210 and 230 nm can be attributed almost entirely to bromide, nitrate, and organic matter, in decreasing order of importance (Ogura and Hanya 1966). The temperature dependence of the absorptivity of sea salt bromide was determined from observations of low-nitrate seawater (NO_3^- < 0.1 µM) at different sample temperatures. Solutions of 840 µM NaBr in DIW were also analyzed to verify that the changes in sea salt absorbance with temperature were primarily due to the changes in the bromide absorptivity. Solutions of 40 µM NO_3^- in DIW and in seawater were also analyzed to determine if nitrate absorptivity exhibited any temperature dependence. We conducted 17 different experiments using eight different ISUS instruments, with both 4- and 1-cm pathlength ISUS probe tips and sample temperatures ranging from 2.8 to 34.2°C.

The data from both 1- and 4-cm pathlength ISUS scans at varying sample temperatures were combined after dividing absorbances with the 4-cm pathlength by 4 to normalize to a 1-cm pathlength. The baseline corrected absorbances were normalized to a salinity of 35 using $A_{35} = A_s/S \times 35$, where A_{35} is the calculated absorbance at a salinity of 35 and A_s is the seawater absorbance at salinity S.

The temperature dependence of the sea salt absorbance is illustrated in Figure 2, which is a compilation of 12 experiments. The baseline-corrected seawater absorbances within 217.0–217.3 and 224.8–225.2 nm wavelengths range increase at higher sample temperature (Figure 2A), whereas the absorbances of 40 µM NO_3^- standards made up in DIW (five experiments) do not show a temperature dependence (Figure 2B).

The seawater absorbances show a strong temperature dependence because they are dominated by the bromide UV absorbance. The temperature slopes of the sea salt spectra were the same as the slopes generated from NaBr solutions with similar Br^- concentrations. The absorption spectrum of aqueous bromide in the deep UV is created by a charge transfer to solvent complex. The interaction of ion and solvent creates a strong temperature dependence (Jortner et al. 1964). Nitrate, on the other hand, has no discernable temperature dependence because its absorption is due to a $\pi \rightarrow \pi^*$ transition that occurs entirely within the molecule (Mack and Bolton 1999). The relatively larger scatter in the nitrate absorbance is probably due to the wider wavelength range used. Laboratory measurements by Zielinski et al. (2007) also found a similar strong temperature dependence of seawater absorbances.

Temperature correction algorithm—The baseline-corrected (240–260 nm linear regression) seawater standard absorbances normalized to a salinity of 35.0 were compiled (n = 2200 data

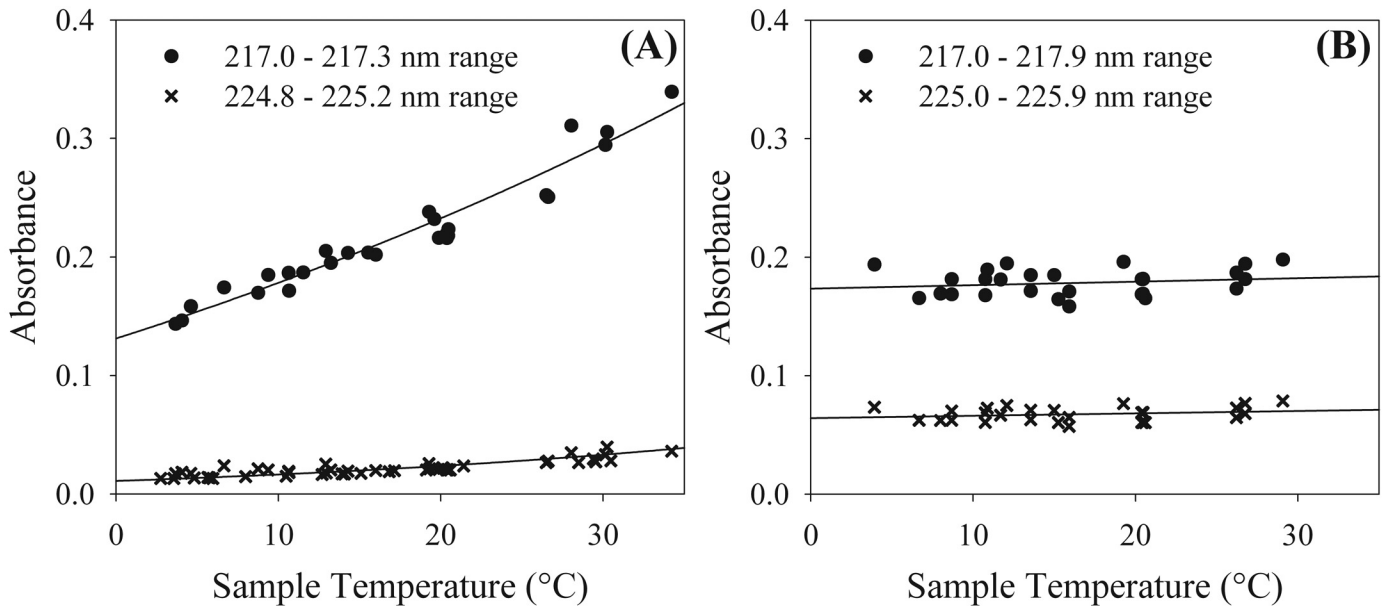

Fig. 2. (A) Seawater absorbance (normalized to salinity 35.0) as a function of sample temperature in two wavelength ranges: 217.0–217.3 and 224.8–225.2 nm. The solid lines are plots of calculated absorbances based on Equation 4. (B) The absorbances of 40 µM NO_3^- in DIW standard as a function of temperature in two wavelength ranges: 217.0–217.9 and 225.0–225.9 nm. The solid lines are the linear regressions of absorbance versus temperature. The 217.0–217.9 nm regression has $y = 0.0003x + 0.17$, $r^2 = 0.042$, and the 225.0–225.9 nm regression has $y = 0.0002x + 0.064$, $r^2 = 0.052$.

points), and a nonlinear multiple regression was calculated using Systat (v. 10; Systat Software, Inc., Chicago, IL, USA). The data in the wavelength range 214–240 nm were fitted with the function:

$$ASW_{(\lambda,T)} = (A + B\times T) \times \exp((C + D\times T) \times (W)) \quad (4)$$

where $ASW_{(\lambda,T)}$ is the baseline-corrected seawater absorbance normalized to a 1-cm pathlength and a salinity of 35.0, λ is wavelength in nm, T is the sample temperature in °C, and W is the wavelength minus 210 nm (for scaling purposes). The resultant regression parameters A, B, C, and D are 1.1500276, 0.02840, –0.3101349, and 0.001222, respectively. Absorbances calculated at 217 and 225 nm using Equation 4 are shown as the solid lines in Figure 2A. Regression of the measured seawater absorbances versus the calculated absorbances at the same temperature and wavelength using Equation 4 gives r^2 = 0.99 and a standard error of the estimate for regression of 0.0056 absorbance units.

To use Equation 4 to temperature-compensate the computation of nitrate, we calculate a temperature-corrected sea salt extinction coefficient at each wavelength ($ESW_{(\lambda,Tis)}$) as follows:

$$ESW_{(\lambda,Tis)} = \frac{ESW_{(\lambda,Tcal)} \times ASW_{(\lambda,Tis)}}{ASW_{(\lambda,Tcal)}} \quad (5)$$

where $ESW_{(\lambda,Tcal)}$ comes from the instrument's calibration file at the known calibration temperature. The two ASW values are calculated at the in situ seawater temperature and the calibration temperature using Equation 4.

At this point, the temperature-corrected $ESW_{(\lambda,Tis)}$ values could be used with the $ENO_3^-{}_{(\lambda)}$ values obtained during each instrument's calibration to calculate nitrate and an optical salinity value by multiple regression using Equation 3. The nitrate values obtained with the temperature-corrected ESW values are moderately more accurate than values computed using non–temperature-compensated values. The salinities derived in this manner are much more accurate. For example, if an instrument is calibrated near 20°C, the temperature slope of Equation 4 will cause non–temperature-compensated values for salinity to be ~23% too low in samples near 10°C.

Once the temperature corrected $ESW_{(\lambda,Tis)}$ values are known, it should be possible to subtract the bromide component before computing nitrate as noted by Zielinski et al. (2007). In this case, the expected spectral component due to sea salt at the in situ temperature ($ASE_{(\lambda,Tis)}$) can be calculated using the observed salinity S (acquired from associated CTD data) with the following equation:

$$ASE_{(\lambda,Tis)} = ESW_{(\lambda,Tis)} \times S \quad (6)$$

This expected spectrum due to sea salt at the in situ temperature is then subtracted from the measured in situ absorption spectrum ($ASM_{(\lambda,Tis)}$) to give the spectrum A' due to NO_3^- and the combined near-linear spectrum produced by DOC and instrument baseline drift at wavelengths within the fit range (217–240 nm for 1-cm pathlength; 220–245 for 4-cm pathlength):

$$A'_{(\lambda)} = ASM_{(\lambda,Tis)} - ASE_{(\lambda,Tis)} \quad (7)$$

Nitrate can then be calculated by

$$A'_{(\lambda)} = e + f\times \lambda + NO_3^- \times ENO_3^-{}_{(\lambda)} \quad (8)$$

where e, f, and NO_3^- are fitted parameters. As noted below, this produces a major improvement in accuracy.

These calculations are independent of the pathlength of the optics because changing pathlength affects both values of ASW in Equation 5 and the changes cancel out. The ESW and ENO_3^- values for each instrument still need to be determined in case of variations in pathlength or wavelength registration; however, calibrations need to be done at only one temperature.

To test the impacts of temperature compensation and removal of the salinity component on the accuracy of the ISUS output and to verify that the temperature correction algorithm is applicable across a wide variety of temperatures, comparisons of computed ISUS nitrate values and corresponding discrete samples analyzed for nitrate concentrations were made for deployments in a variety of conditions. Nitrate concentrations were calculated under the following three conditions: (*a*) without any temperature compensation of the sea salt absorption coefficient and fitting both salinity and nitrate using Equation 3; (*b*) recalculating the sea salt extinction coefficient using the sample temperature and then fitting both salinity and nitrate using Equation 3; or (*c*) recalculating the sea salt extinction coefficient using the sample temperature, subtracting the expected absorbance due to the CTD measured salinity at that temperature, and then calculating the nitrate concentration using Equation 8. In the rest of this article, the first algorithm will be referred to as NTC (no temperature compensation), the second as TCSV (temperature compensated, salinity variable), and the third as TCSS (temperature compensated, salinity subtracted).

ISUS nitrate data from a variety of deployments were calculated using the above three algorithms and are plotted in Figure 3 versus nitrate in corresponding discrete water samples that were collected, frozen, and then analyzed using standard wet chemistry methods with an Alpkem Rapid Flow Analyzer (RFA) instrument (Sakamoto et al. 1990). Of these samples (n = 182), 62 are from the ISUS deployed on CTD profiling casts done in eastern Pacific (34.0°N, 129.0°W) oligotrophic waters with temperatures ranging from 9.3 to 19.4°C, salinities ranging from 33.3 to 33.8, and nitrate ranging from essentially zero to 20 µM. The surface waters at this station contain no nitrate detectable with the RFA analysis down to a depth of 110 m. Sixty-three of the samples are from the Southern Ocean with temperatures ranging from –1.7 to 7.1°C, salinities ranging from 33.7 to 34.7, and nitrate ranging from 21.3 to 34.5 µM. Forty-two samples are from four casts done off the central California coast (Monterey Bay) with temperatures

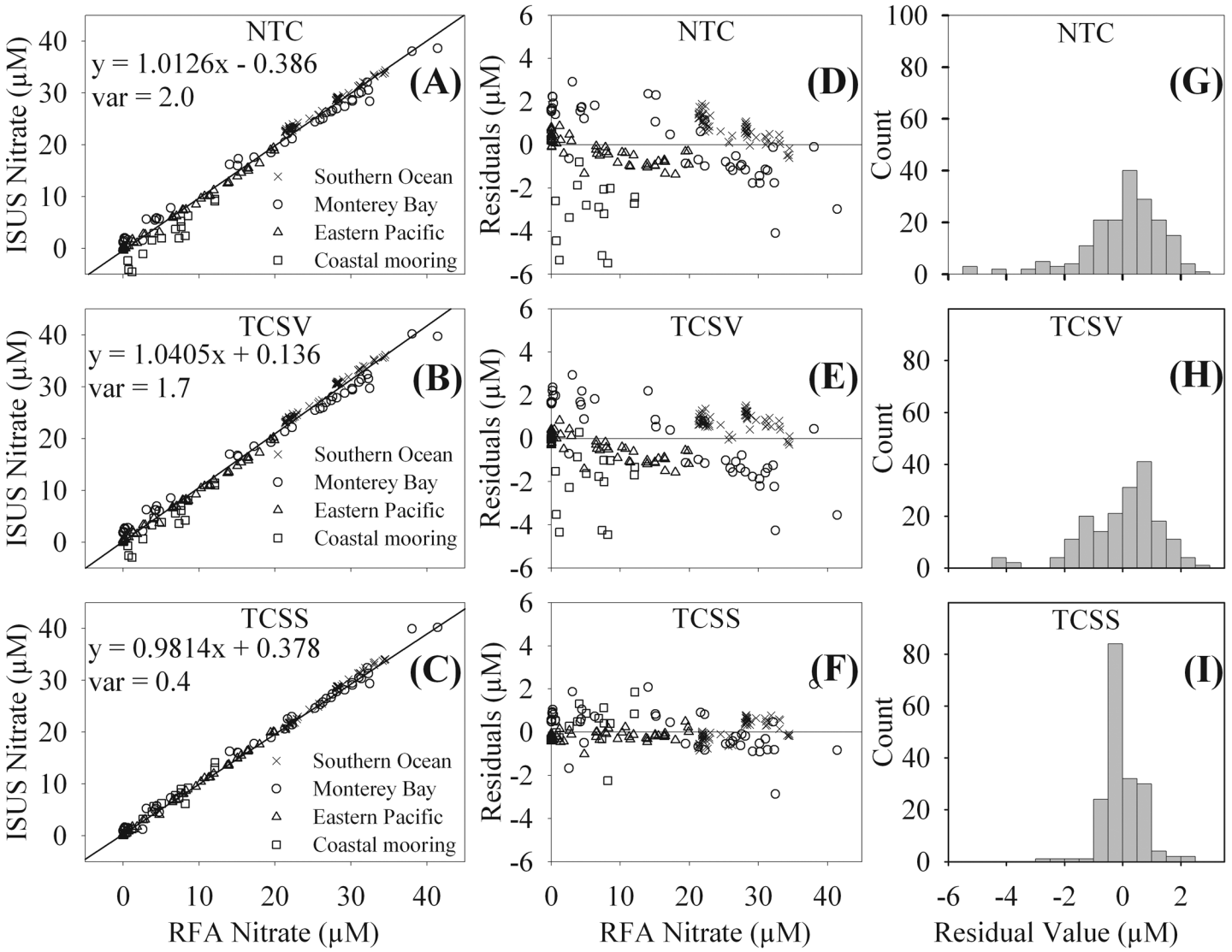

Fig. 3. (A–C) Regression plots and parameters for the regression of ISUS nitrate concentrations versus discrete nitrate samples using 3 different calculation algorithms. (D–F) Plots of the residuals of the regression (n = 182). (G–I) Histogram plots of the residuals of the regression.

ranging from 6 to 14.5°C, salinities ranging from 33.2 to 34.3, and nitrate ranging from 0.05 to 41.4 µM. Fifteen of the samples are from a 1-year mooring deployment off the central California coast (36.756°N, 122.034°W) with temperatures ranging from 11.5 to 14.8°C, salinities ranging from 32.4 to 33.7, and nitrate ranging from 0.6 to 12.1 µM.

Figure 3A–C shows the regression plots and parameters for the ISUS nitrate versus discrete nitrate concentrations using the three different algorithms. The regression residuals are plotted versus RFA nitrate concentration in Figure 3D–F. The histogram of the regression residuals is shown in Figure 3G–I. Without using any temperature compensation, there is a good correlation between the ISUS and RFA nitrate concentrations (correlation coefficient, r^2 = 0.99). The standard error of the estimate for regression is 1.4 µM, which corresponds to a variance of 2.0 µM^2. Note, however, that there are several samples at low RFA nitrate concentrations that the NTC algorithm calculates as negative nitrate concentrations.

The TCSV algorithm also shows a good correlation between the ISUS and RFA nitrate concentrations (r^2 = 0.99). The standard error of the estimate for regression improves to 1.3 µM, which corresponds to a variance of 1.7 µM^2. There are still some negative outliers, however, as seen in Figure 3 G–I. The standard error of the estimate for regression with the TCSS algorithm is further reduced to 0.65 µM, which corresponds to a variance of 0.4 µM^2 (r^2 = 0.99). With the TCSS algorithm, there are no negative nitrate concentrations larger than –0.05 µM and the variance has been improved 5-fold compared with the NTC algorithm. The histogram of the residuals shows greatly reduced scatter compared with the other algorithms.

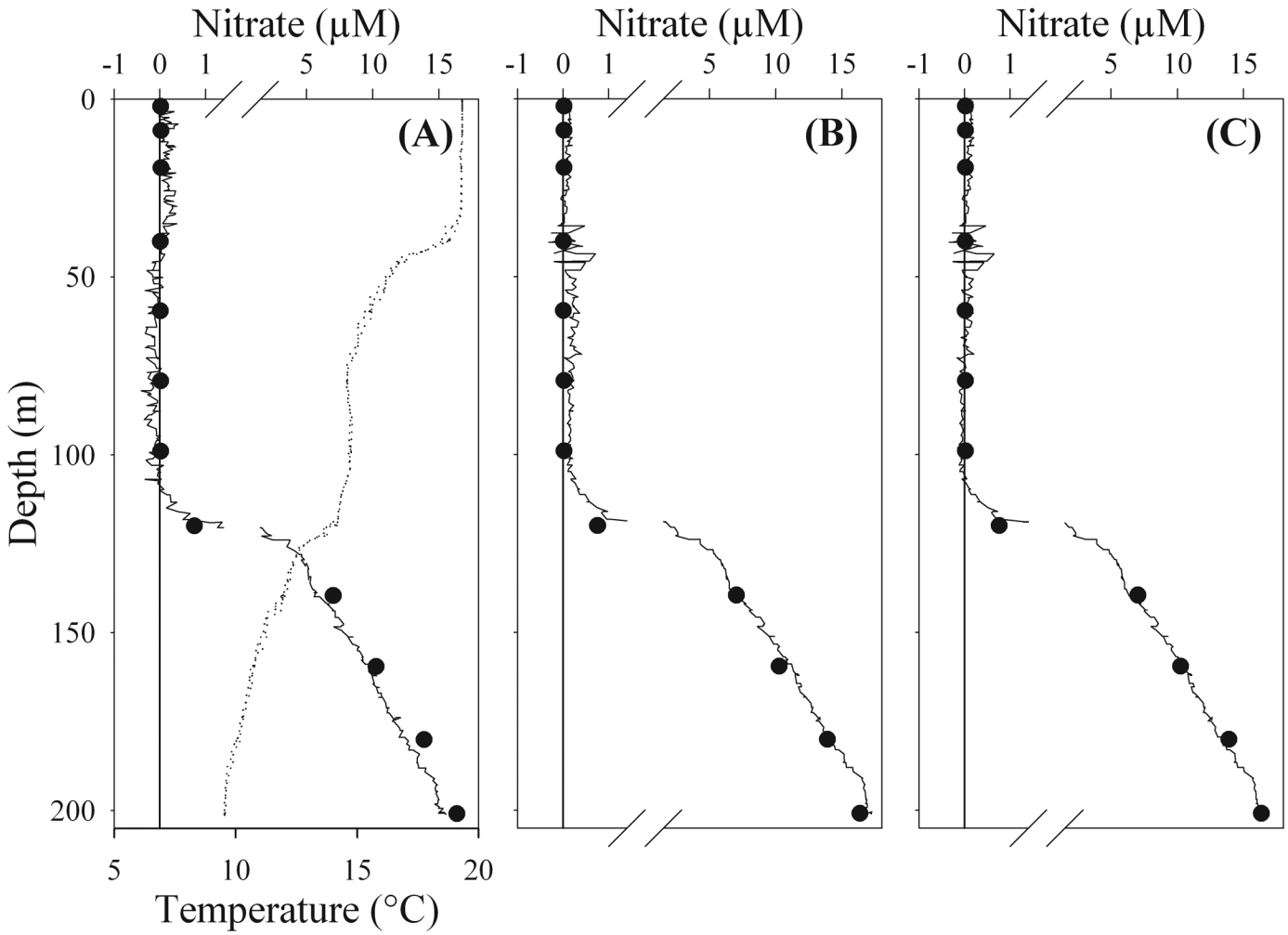

Fig. 4. Profiles of ISUS nitrate (µM) concentrations (solid line) calculated under three conditions versus depth (m) at an eastern Pacific (34.00°N, –129.00°W) oligotrophic station. (A) NTC. (B) TCSV. (C) TCSS. The discrete nitrate samples are shown as black circles. The CTD temperature (°C) profile is shown as a dotted line in (A) but is the same across all panels. Note the axis break for nitrate at 1.2 µM.

Profiling cast in eastern Pacific oligotrophic waters—A CTD profiling cast done with an ISUS attached to the rosette in eastern Pacific (34.0°N, 129.0°W) oligotrophic waters is shown in Figure 4. Note the break in the nitrate axis at 1.2 µM. The ISUS data are from the downcast profile. The ISUS generates a datapoint once every 1.7 s, which provides 0.3-m resolution at the descent rate of 20 m min^{-1}. The nitrate concentrations in the upper 110 m were essentially zero.

The NTC algorithm gives nitrate values that are slightly negative in the 50–105 m depth range as temperatures decrease below the thermocline (Figure 4A). The average ± standard deviation of the ISUS values in this 50–105 m depth range is –0.14 ± 0.11 µM. The ISUS nitrate values also have a negative bias in the deeper cold waters.

The nitrate concentrations calculated with the TCSV algorithm (Figure 4B) lack the negative concentrations in the 50–105 m depth range, but the concentrations appear to be slightly biased on the high side. The average ± standard deviation of the ISUS values in the 50–105 m depth range with this algorithm are 0.18 ± 0.09 µM.

The nitrate values calculated with the TCSS algorithm (Figure 4C) match the discrete samples very closely. The average ± standard deviation of the ISUS values in the 50–105 m depth range with this algorithm are –0.008 ± 0.08 µM.

The small nitrate features at ~40–45 m (Figure 4B and C) is probably due to a mismatch of the CTD temperature and the ISUS sample temperature at the depth of the maximum temperature gradient. This feature does not appear in the data that is not temperature-compensated and illustrates the importance of precisely matching the in situ temperature in areas of strong thermal gradients.

Central California Monterey Bay M1 mooring data—Data from a 1-year deployment of an ISUS sensor on a mooring in Monterey Bay, CA, are shown in Figure 5. The top panel shows the temperature and salinity data at ~1 m. The ISUS nitrate values calculated with the NTC algorithm (Figure 5B) show a tendency

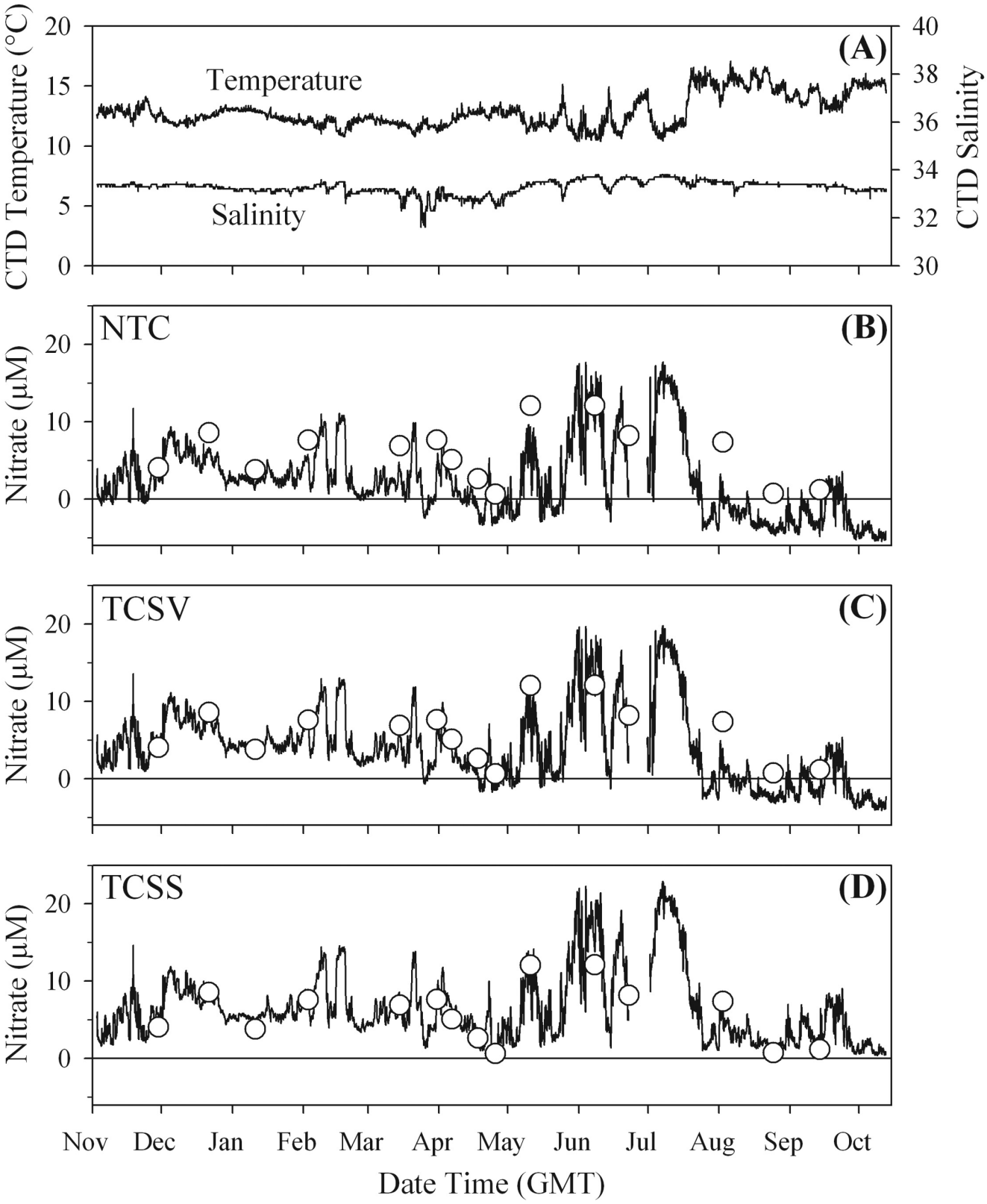

Fig. 5. Four-panel plot of data from a 1-year deployment on a mooring in Monterey Bay (36.756°N, 122.03°W). (A) Surface CTD temperature (°C) and salinity. (B) NTC. (C) TCSV. (D) TCSS. The open circles are nitrate values (µM) from discrete samples collected in close proximity to the mooring.

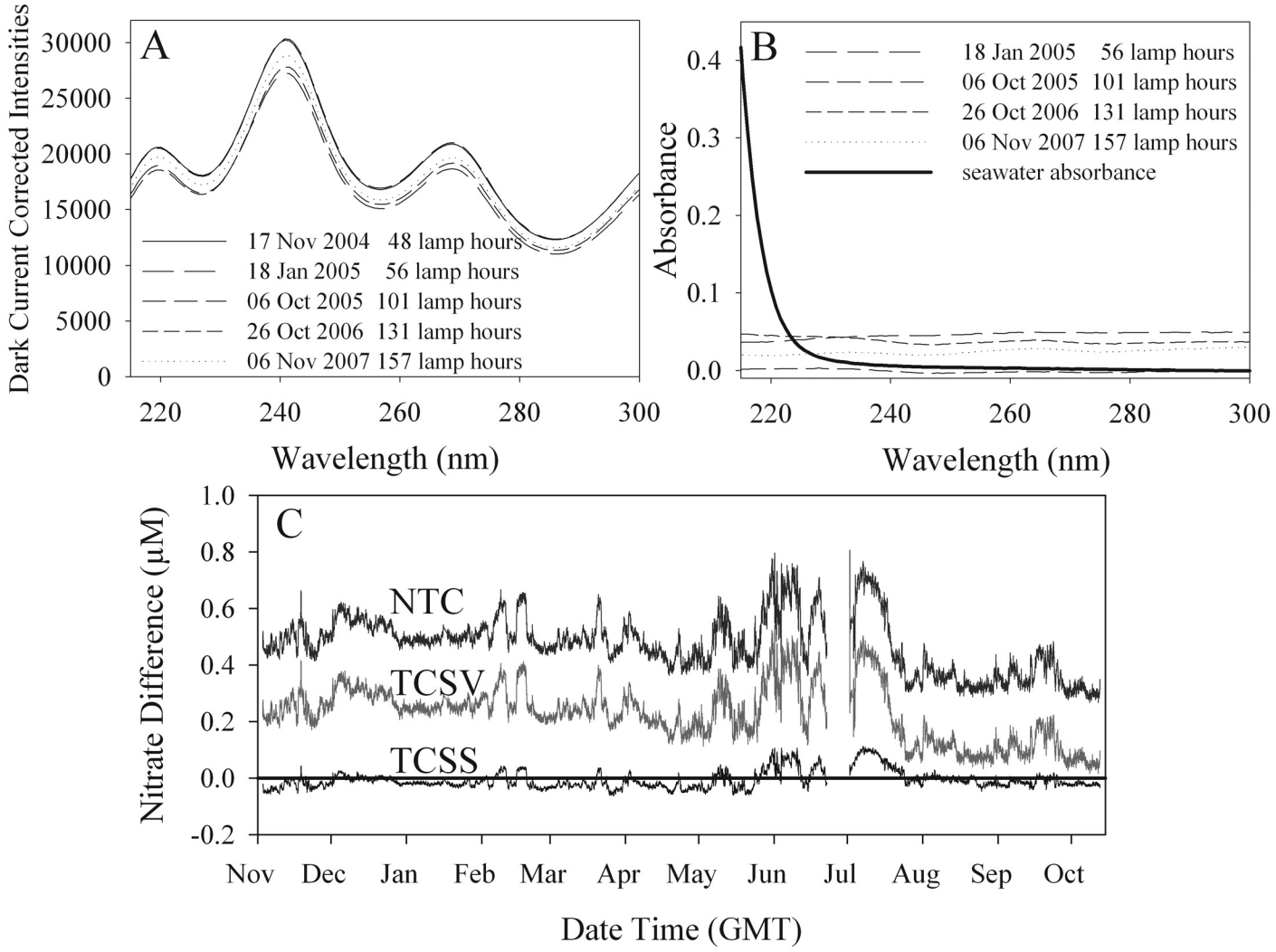

Fig. 6. (A) Dark current–corrected intensities of DIW from five calibrations of an ISUS instrument with the date of the calibration and cumulative lamp hours in the legend. (B) The absorbances of DIW from the calibrations calculated relative to the initial DIW scan measured on 17 November 2004 and a seawater scan. (C) The differences between the nitrate concentrations (µM) from the data shown in Figure 5 calculated with the 26 October 2006 calibration minus the 6 October 2005 calibration.

to drift toward negative nitrate values over time, with calculated concentrations approaching –5 µM at the end of the deployment. The negative values associated with times of low nitrate concentration are the source of the large negative points plotted in Figure 3B and D.

Using the TCSV algorithm (Figure 5C) gives a much better match throughout the data record, but there are still some negative values predicted by ISUS during the last 3 months of the deployment. Calculations using the TCSS algorithm (Figure 5D) result in excellent agreement with the discrete data, and the values at the end of the deployment are no longer negative.

Impacts of long-term drift—The effects of long-term drift in lamp output on calculated nitrate may also be reduced using the TCSS algorithm. We assessed this by using calibration files prepared over a 3-year period to compute the nitrate concentrations from the UV spectra measured on the M1 mooring. This is the same data set shown in Figure 5. Changes in the dark current–corrected intensities of the DIW scans over time from calibrations of this ISUS are shown in Figure 6A. These dark current–corrected DIW intensities are from five calibrations spanning 3 years of deployments. After an initial 48-h lamp burn in period, this instrument was first calibrated on 17 November 2004 and then deployed on a mooring in Elkhorn Slough, CA (LOBO L01 mooring), for approximately 1 year with one recalibration done on 18 January 2005. The instrument was then recalibrated on 6 October 2005 before deployment on the Monterey Bay M1 mooring for another year that

generated the data shown in Figure 5. The instrument was subsequently recalibrated on 26 October 2006 and redeployed on the LOBO L01 mooring for another year and then recalibrated on 6 November 2007 and is currently deployed on the LOBO L01 mooring.

The DIW absorbances calculated relative to the initial DIW intensities measured on 17 November 2004 from these calibrations are shown in Figure 6B. A typical seawater scan from a calibration is also plotted. In this instrument, although there are small shifts in the baseline absorbance over time, they are primarily linear baseline shifts that do not have an appreciable effect on the calculated nitrate concentration, as any linear shifts are compensated by the *e* and *f* parameters in Equation 3. Because the calculations use the best fit over a range of wavelengths and not just a single wavelength, linear shifts in the baseline up or down do not affect the calculated concentrations, as they do not affect the shape of the spectra.

Small changes in spectral shape that do appear as lamps age are largely corrected with the TCSS algorithm. For example, the differences between nitrate concentrations calculated with the post deployment 26 October 2006 calibration minus nitrate concentrations calculated with the predeployment 6 October 2005 calibration for the Monterey Bay mooring data from Figure 5 are shown in Figure 6C. The average ± standard deviation of these differences was 0.48 ± 0.1 µM NO_3^- for NTC, 0.23 ± 0.1 µM NO_3^- for TCSV, and –0.0064 ± 0.03 µM NO_3^- for TCSS. The increase in accuracy achieved with using the temperature-correction algorithm coupled with subtracting the salinity component reduced any changes due to baseline drift from lamp aging over the course of 1 year.

This ISUS was deployed for another year on the LOBO L01 mooring and then recalibrated on 6 November 2007. The differences between nitrate concentrations calculated with this 6 November 2007 calibration minus the nitrate concentrations calculated with the predeployment 6 October 2005 calibration were –2.2 ± 0.09 µM NO_3^- for NTC, –2.5 ± 0.1 µM NO_3^- for TCSV, and 1.1 ± 0.09 µM NO_3^- for TCSS.

Error reduction by reducing the terms in the fitting model—The improvement in accuracy of the computed nitrate values that arises when the spectral signal due to bromide is removed from the fit occurs because the NO_3^- and Br^- spectra are relatively colinear (Johnson and Coletti 2002). Small spectral errors may be produced by a variety of processes. These include fouling of the optics that does not shift the baseline by a constant amount, long-term drift of the lamp output that is not a constant proportion at each wavelength, or changes in lamp output due to variable temperature. In each of these cases, systematic errors will result when Equation 3 is applied to estimate nitrate from the observed spectra. This may create a situation where the best fit to the observed UV spectrum will result by making the salinity component too high and nitrate too low, or vice versa. These compensating errors offset each other and produce a best spectral fit to the absorbance model. By subtracting the salinity spectrum, it is no longer possible to have offsetting errors in nitrate and salinity, and the computed nitrate will be more accurate. This process is illustrated by considering a plot of optical nitrate versus optical salinity in the upper 100 m from eastern Pacific oligotrophic waters (Figure 7). These data are well above the nitracline at 120 m in water containing essentially zero nitrate and an average salinity of 33.5, which is indicated by the solid vertical lines. Temperature is 19.4°C in the upper 45 m and drops to 15°C at 100 m. The NTC algorithm yields calculated optical nitrate and optical salinity, which covary in the upper 45 m where there is little temperature change (open triangles). Temperature drops 4°C in the 45–100 m depth range, and the salinity estimated from the UV spectrum drops markedly due to the temperature dependence of the bromide spectrum, whereas there is little change in computed nitrate.

The salinity calculations are much improved with the TCSV algorithm, but there is now a strong negative correlation between computed nitrate and salinity from the surface to 110 m. The best fits to the observed spectra are often produced with too low a salinity value and too high a nitrate value. The TCSS algorithm eliminates the possibility for compensating errors. The scatter in the calculated nitrate values is lower and the accuracy is greatly improved by correcting values such as –0.4 µM NO_3^- obtained with the TCSV algorithm, up to their expected values (Figure 7C). Subtracting the sea salt spectra with the observed salinity reduces the degrees of freedom in the fit and prevents compensating errors from occurring. This improvement in accuracy can occur whenever there are offsetting errors in nitrate and salinity. These offsetting errors result when Equation 3 does not fully describe the observed spectra. This may occur when there is a mismatch in the calibration temperature and the in situ temperature, and when small amounts of fouling on the optics or long-term drift bias the accuracy of the computed absorbance values.

Discussion

The new algorithm has been tested in waters ranging from the Southern Ocean to the oligotrophic Pacific and works in all of these diverse locations. By reducing the degrees of freedom in calculating nitrate concentrations, the accuracy of the ISUS instrument has been substantially improved. There is a greater than 2-fold reduction in the standard error of the estimate for regression from 1.4 to 0.65 µM (Figure 3A–C), which corresponds to a 5-fold reduction in variance (Figure 3G–I). The large reduction in variance corresponds to significantly fewer (*F*-test; $P < .001$) large residuals as shown by the histogram plots. Improvement in accuracy using the TCSS algorithm in a moored application resulted in the elimination of the negative (to –4.5 µM NO_3^-) values that are computed in the non–temperature-compensated case. Incorporating the CTD temperature and salinity measurements can help to compensate for drift errors and will allow the use of this instrument in a wide range of locations for long-term in situ measurements. The elimination of large, negative nitrate estimates

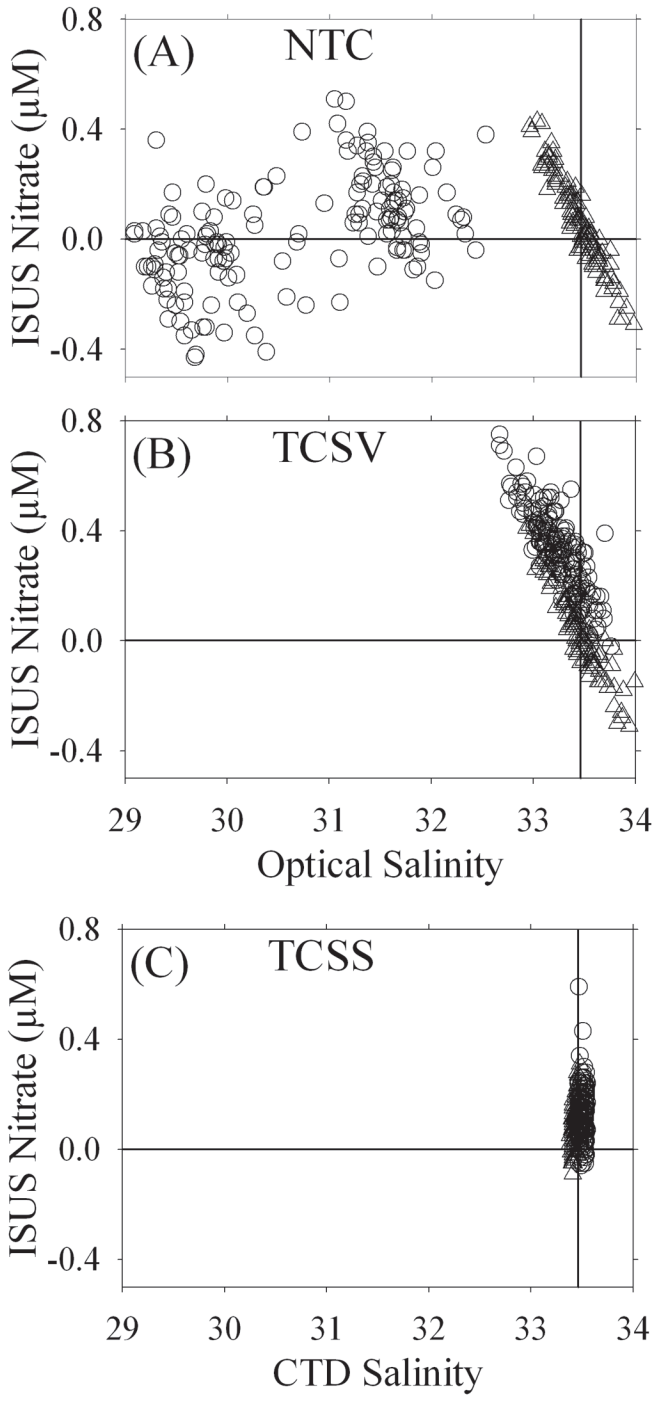

Fig. 7. Optical nitrate (µM) versus optical salinity in the upper 100 m at an oligotrophic eastern Pacific station calculated with NTC (A), TCSV (B), and TCSS (C). Triangles are from the surface down to 45 m (19.4–18.5°C), and the circles are from 45 to 100 m (18.5–14.6°C). The seawater at this station at this station contains essentially zero nitrate down to a depth of 110 m.

transforms ISUS data obtained on long-term deployments from a relative indicator of nitrate to a sensor with absolute accuracy that begins to approach laboratory methods.

A drawback to using this algorithm is that a CTD with a sampling frequency at least as fast as the ISUS needs to be deployed in the same location. In our deployments, this has not been an issue because the CTD data are necessary to put the nitrate data into oceanographic context. To generate real-time concentrations of the highest accuracy, the ISUS instrument controller software must be modified so that the CTD data are passed to it before the concentration calculations are made. The TCSS algorithm can be used to postprocess data that have already been collected, as well. In the event that the CTD instrument ceases to work properly, the ISUS instrument can still generate reasonable concentrations, but some accuracy may be lost.

The characterization of the spatial and temporal variability of nitrate is greatly enhanced by this ability to measure concentrations without chemical manipulation and with a temporal resolution of approximately 1 s. The ability to capture episodic events bringing nitrate into the mixed layer and measuring nitrate consumption via deployments on remote platforms such as Argo floats and long-range AUVs will be a very powerful tool to use in assessing nitrogen dynamics. The capability to measure nitrate with high temporal resolution will enable a variety of measurements, such as measuring thin layers in profiling casts and eddy-correlation measurements of nitrate fluxes at the sediment/water interface.

References

Johnson, K. S., and L. J. Coletti. 2002. In situ ultraviolet spectrophotometry for high resolution and long-term monitoring of nitrate, bromide and bisulfide in the ocean. Deep-Sea Res. I 49:1291-1305.

Johnson, K. S., L. J. Coletti, and F. P. Chavez. 2006. Diel nitrate cycles observed with in situ sensors predict monthly and annual new production. Deep-Sea Res. I 53:561-573.

Jortner, J., M. Ottolenghi, and G. Stein. 1964. On the photochemistry of aqueous solutions of chloride, bromide, and iodide ions. J. Phys. Chem. 68:247-255.

Mack, J., and J. R. Bolton. 1999. Photochemistry of nitrite and nitrate in aqueous solution: a review. J. Photochem. Photobiol. A Chem. 128:1-13.

McNeil, J. D., H. W. Jannasch, T. Dickey, D. McGillicuddy, M. Brzezinski, and C. M. Sakamoto. 1999. New chemical, bio-optical and physical observations of upper ocean response to the passage of a mesoscale eddy off Bermuda. J. Geophys. Res. 104:15537-15548.

Ogura, N., and T. Hanya. 1966. Nature of ultra-violet absorption of sea water. Nature 212:758.

Sakamoto, C. M., G. E. Friederich, and L. A. Codispoti. 1990. MBARI procedures for automated nutrient analyses using a modified Alpkem series 300 Rapid Flow Analyzer. Monterey Bay Aquarium Research Institute Tech. Rep. 90-2, 87 pp.

Sakamoto, C. M., D. M. Karl, H. W. Jannasch, R. R. Bidigare, R. M. Letelier, P. M. Walz, J. P. Ryan, and P. S. Polito. 2004. Influence of Rossby waves on nutrient dynamics and the plankton community structure in the North Pacific subtropical gyre. J. Geophys. Res. 109:C05032, doi:10.1029/2003JC001976.

Zielinski, O., B. Fiedler, R. Heuermann, A. Körtzinger, E. Kopiske, G. Meinecke, and K. Munderlow. 2007. A new nitrate continuous observation sensor for autonomous subsurface applications: technical design and first results. Oceans 2007—Europe conference, DOI: 10.1109/OCEANSE.2007.4302300.

Submitted 16 July 2008
Revised 17 November 2008
Accepted 30 December 2008